Austenite Stability and Strain Hardening in C-Mn-Si Quenching and Partitioning Steels

Metallurgical and Materials Transactions A
01/16/2019

AUTHORS

Christopher B. Finfrock (Corresponding Author) [1]
PhD Student
cfinfroc@mines.edu
360-305-9821

Amy J. Clarke[1]
Associate Professor
amyclarke@mines.edu

Grant A. Thomas[2]
Manager, Product Research
grant.thomas@aksteel.com

Kester D. Clarke[1]
Assistant Professor
kclarke@mines.edu

[1]Colorado School of Mines
Advanced Steel Processing and Products Research Center
1500 Illinois St
Golden, CO 80401

[2]AK Steel Corporation
Steel Research & Innovation Center
9227 Centre Pointe Drive
West Chester, Ohio 45069

ORIGINALITY STATEMENT

The authors confirm that the results reported in the manuscript are original and neither the entire work, nor any of its parts, have been previously published. The authors confirm that the article has not been submitted to peer review, nor has been accepted for publishing in another journal. The authors confirm that the research in their work is original, and that all the data given in the article are real and authentic.

ABSTRACT

Quenching and partitioning (Q&P) processing of third generation advanced high strength steels generates multiphase microstructures containing metastable retained austenite. Deformation-induced martensitic transformation of retained austenite improves strength and ductility by increasing instantaneous strain hardening rates. This paper explores the influence of martensitic transformation and strain hardening on tensile performance. Tensile tests were performed on steels with nominally similar compositions and microstructures (11.3 to 12.6 volume percent retained austenite and 16.7 to 23.4 volume percent ferrite) at 980 and 1180 MPa ultimate tensile strength levels. For each steel, tensile performance was generally consistent along different orientations in the sheet relative to the rolling direction, but a greater amount of austenite transformation occurred during uniform elongation along the rolling direction. Neither the amount of retained austenite prior to straining, nor the total amount of retained austenite transformed during straining could be directly correlated to tensile performance. It is proposed that stability of retained austenite, rather than austenite volume fraction, greatly influences strain hardening rate, and thus controls strength and ductility. If true, this suggests that tailoring austenite stability is critical for optimizing the forming response and crash performance of quenched and partitioned grades.

I. INTRODUCTION

Advanced high strength steels (AHSS) are of rapidly increasing commercial interest[1], due to increasing global automobile production and heightened requirements for improved passenger safety and fuel efficiency[2]. Third generation AHSS are attractive, particularly due to their enhanced mechanical properties relative to first generation AHSS and lower cost than second generation AHSS[3]. Due to their enhanced ductility and strength, third generation AHSS can be used in thinner gauges, reducing body-in-white weight and consequently improving fuel efficiency. Unlike conventional automotive sheet steels, AHSS achieve improved ductility by suppressing strain localization with transformation-induced plasticity (TRIP)[4–7]. In practice, a well-documented increase in tensile elongation occurs because of deformation-induced transformation from metastable austenite to martensite[8–10].

Quenching and partitioning (Q&P) processing, initially proposed by Speer *et al.*[11–14], has been used to create steel microstructures that take advantage of TRIP by containing small fractions of retained austenite that are thermally stable at room temperature. In addition, these microstructures contain large volume fractions of martensite, such that the yield strength is comparable to martensitic steels. Functionally, the yield strength is controlled largely by the presence of martensite, while work hardening and ductility are enhanced by TRIP.

Many Q&P compositions contain carbon[15] for austenite stabilization, manganese[16,17] for austenite stabilization and solid solution strengthening, and silicon[18] to suppress the formation of carbides, which may otherwise reduce austenite stability by depleting carbon in austenite. By modifying either composition or Q&P heat treatment parameters, the microstructure and mechanical stability of retained austenite can be tailored, with the intention of optimizing deformation behavior.

The role of austenite transformation on strain hardening rate is of particular interest for suppression of strain localization[19,20]. Strain hardening has been characterized for individual phases in Q&P steels, with the assumption that Q&P steels behave as composite materials[21–23]. In Q&P processed material, strain hardening behavior has been explored in martensite[24] and retained austenite[25]. Similar work has been performed for other AHSS, including manganese-enriched TRIP grades[26]. Deformation processing factors[4, 9,10,27-29], such as strain rate, strain state, and temperature, as well as microstructure factors[30], such as distribution of carbon[31], presence of carbides[32,33], phase volume fractions[34,35], austenite grain size and morphology[36-39], and strain partitioning[40-43], have all been proposed as levers that affect the stability of retained austenite.

A simplistic design approach for AHSS that contain austenite for TRIP-enhanced ductility is to maximize the volume fraction of retained austenite; Wang *et al.* stated that strength/elongation product increases linearly with respect to austenite volume fraction[44]. However, an exhaustive review by De Moor *et al.* showed that no clear correlation exists between the amount of retained austenite before deformation and total elongation or strength/elongation product[45]. More recent works have investigated such behavior in TRIP steels[46, 47], Medium-Mn steels[48], and Q&P steels[49-52]. Most authors suggest that solely maximizing austenite fraction is inadequate for achieving the best possible tensile properties; rather, the austenite stability must be controlled by tailoring the microstructure by means discussed previously[30-43]. The consensus in recent literature is that promoting progressive transformation of retained austenite during deformation is critical for achieving optimal mechanical properties; a microstructure which facilitates extensive transformation of austenite across a broad range of strains will exhibit high work hardening rates that improve formability and suppress strain localization[26, 34, 53, 54]. It is hypothesized that a microstructure optimized for progressive transformation should contain austenite with a spectrum of stabilities.

This paper aims to further clarify the relationship between austenite stability, austenite volume fraction, and tensile mechanical performance in industrially produced Q&P steels[55-57]. Steels created with slightly different Q&P processing parameters and otherwise similar chemistries and microstructures are evaluated to study how small process variations, inherent in large-scale mill environments, can influence austenite stability and tensile performance. Orientation dependence of TRIP with respect to the rolling direction is examined, with the hypothesis that crystallographic texture and local austenite stability variations within the sheet could impact TRIP.

II. EXPERIMENTAL PROCEDURE

Q&P steels were manufactured on commercial scale production equipment. The steels were designed to have ultimate tensile strengths of 980 and 1180 MPa. Both strength levels of steel were intercritically annealed to form approximately 20 percent intercritical ferrite. Variants of the same strength level (e.g. QP980-A and QP980-B) exhibited nearly identical prior austenite grain size. After intercritical annealing, samples of each strength level were subsequently processed by two distinct Q&P processing routes; the resulting variants are referred to hereafter as QP980-A, QP980-B, QP1180-A, and QP1180-B. The specific Q&P processing parameters used to create these steels are proprietary and correspondingly omitted from this paper.

Chemical composition analysis was performed using LECO chemical analysis and by chemical spectroscopy. As shown in Table I, the steels contain similar amounts of carbon and silicon, while the QP1180 steels contain a greater amount of manganese. The A and B variants of each steel have slightly different austenite and ferrite volume fractions. Since ferrite, retained austenite, and martensite are the predominant phases in the microstructures, it is inferred that the martensite occupies the remainder of the sample volume not occupied by either ferrite or retained austenite.

Sheet-type tensile specimens, with geometries conforming to ASTM E8[58], were removed from each material in orientations of 0°, 45°, and 90° with respect to the rolling direction. The geometry of the tensile specimens is shown schematically in Figure 1. Four replicates of each sample condition were strained at a rate of 0.05 min^{-1} (0.00083 s^{-1}) to failure. A screw-driven MTS Alliance RT/100 tensile frame, equipped with an MTS 20,000 lbf load cell and a two-inch extensometer, was used to collect load-displacement data at a data acquisition rate of 15 Hz. The true instantaneous strain hardening exponent (n_i) was evaluated from 0.01 percent engineering strain until the onset of necking using EQN 1[19]:

$$n_i = \frac{\partial(\ln \sigma)}{\partial(\ln \varepsilon)} \qquad \text{[EQN 1]}$$

where σ and ε are true stress and true strain, respectively. To smooth the n_i versus engineering strain curves, the n_i values were averaged over sixty adjacent n_i values.

Characterization of the Q&P microstructure was performed post-mortem in the unstrained grip section of tensile bars removed from the rolling direction. A section of each steel was mounted and polished, revealing the transverse plane. Samples were then etched with one percent Nital solution for 10 seconds. These metallographic samples were viewed optically and with an electron microscope.

Optical microscopy (OM) was performed using an Olympus PMG 3 inverted microscope. Polarizing optics were used to increase color contrast between phases, such that ferrite appeared blue while martensite appeared orange or brown. ImageJ color thresholding was used to measure the area fraction of blue ferrite phase existing on ten images (100x magnification) of each steel. Scanning electron microscopy (SEM) was performed using an FEI Quanta 600 environmental scanning electron microscope (ESEM) in the secondary electron imaging mode.

Retained austenite volume fraction was determined using X-ray diffraction (XRD), by comparing the integrated intensities of diffracted peaks of ferrite and austenite, using the two-peak method outlined in ASTM E975[59] and theoretical intensity data[60]. A Malvern Panalytical Empyrean diffractometer equipped with a molybdenum X-ray source and a zirconium Kβ-filter was used to perform scans over a 2θ range of 10° to 150° to identify present phases, followed by higher resolution scans over the 2θ range of 21° to 37° to record the α(200), α(211), γ(200) and γ(220) peaks. The molybdenum X-ray tube was chosen to reduce X-ray fluorescence and maximize resolution.

XRD scans were performed on the fractured tensile bars in the unstrained grip section and in the uniformly elongated section. The tensile bars were polished to mirror finish, then subsequently electrochemically thinned to remove any surface deformation layer. Scans were taken along three orientations (Figure 1), parallel, diagonal, and perpendicular to the tensile axis, to mitigate effects of microstructural texture on measured retained austenite volume fraction[61, 62]. Intensities of ferrite and austenite peaks from each orientation were subsequently compared to compute retained austenite volume fraction.

Table I: As-Received Chemical Compositions and Phase Amounts of Q&P Steels

Steel	**Thickness**	**C**	**Mn**	**Si**	**Retained Austenite**	**Ferrite**	**Martensite**
	mm	*wt pct*	*wt pct*	*wt pct*	*vol pct*	*vol pct*	*vol pct*
QP980-A	1.4	0.201	1.93	1.62	11.3 ± 0.5	23.4 ± 3.0	Balance
QP980-B	1.4				11.3 ± 0.2	19.6 ± 2.0	Balance
QP1180-A	1.6	0.204	2.26	1.74	11.4 ± 0.4	21.8 ± 5.7	Balance
QP1180-B	1.6				12.6 ± 0.2	16.7 ± 2.3	Balance

III. RESULTS

A. Microscopy of Q&P Microstructures

Optical microscopy reveals a Q&P microstructure containing light-etching ferrite and dark-etching martensite and retained austenite (Figure 2). Polarized light reveals ferrite as teal blue and martensite and austenite as brown. The area of blue ferrite regions was measured for each steel, with estimated volume percent ferrite shown in Table I. Each steel contains approximately 20 percent intercritical ferrite, with marginally greater amounts of ferrite existing in “A” conditions for both strength levels. Variability of several volume percent existed between images of each steel (Table I).

Scanning electron microscopy reveals a fine microstructure consisting of multiple phases, like those reported in literature[63-66]. Based upon detailed characterization by Navarro-Lopez[66], it is speculated that the dark featureless regions are ferrite (F), blocky regions exhibiting fine internal laths surrounded by white blocks are martensite-austenite islands (MA), and elongated white regions are film-like retained austenite (RA). The microstructures of each steel appear similar (Figure 3).

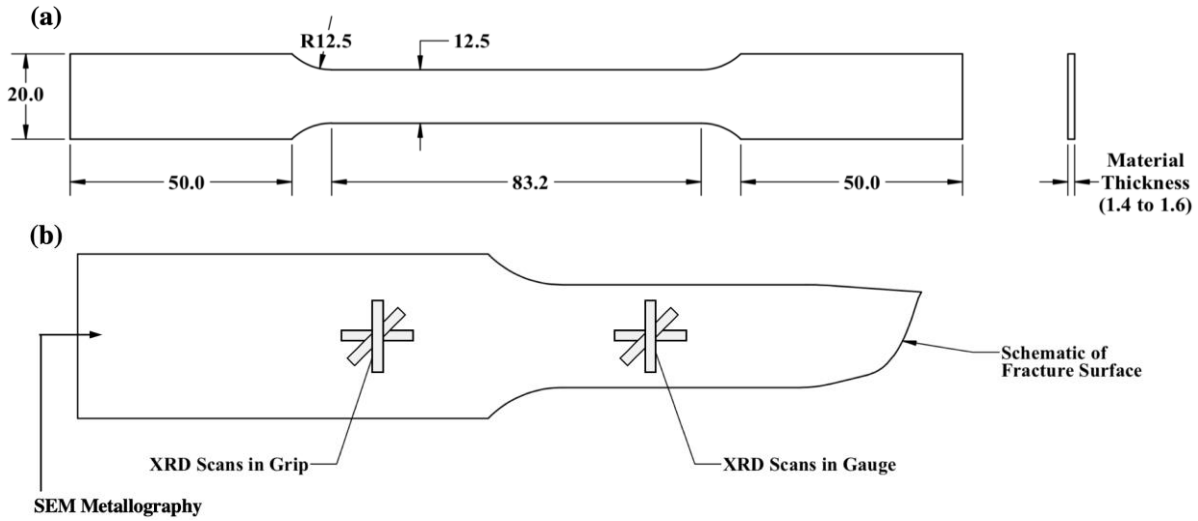

Figure 1: (a) Schematic of tensile specimen geometry with units in millimeters. (b) Location and orientation of XRD scans and SEM metallographic samples removed from the fractured tensile specimens.

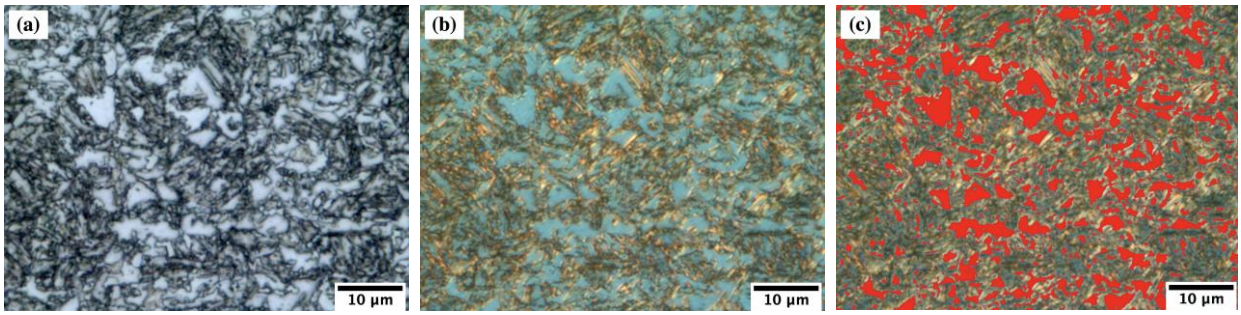

Figure 2: Optical micrographs of QP980-A, (a) in black and white, (b) photographed with polarized light, revealing ferrite as teal blue and martensite and austenite as orange, and (c) color thresholding overlay (red). The region in this image contains 24.0 area percent ferrite, while the average of ten images revealed 23.4 area percent ferrite.

B. Tensile Deformation and Strain Hardening Behavior

Tensile specimens from three orientations (0°, 45°, and 90° with respect to the rolling direction) of each steel were strained to failure. In all four steels, roundhouse yielding occurs at a high yield stress, due to the presence of tempered martensite in the microstructure. Following yielding, the true strain hardening rate reaches a minimum at an engineering strain of approximately 0.02, then increases as tensile strain is increased.

Engineering stress and true instantaneous strain hardening exponent, n_i, are plotted versus engineering strain in Figure 4. Although four replicates of each condition were tested, only one representative replicate of each condition is plotted here, to allow for direct comparison between the tensile deformation

response and austenite transformation for each tensile bar. In QP980-A and QP1180-B, the stress-strain behavior and n_i curves are consistent regardless of orientation (0°, 45°, or 90°). Correspondingly, each orientation had a very similar uniform elongation. However, in QP980-B and QP1180-A, work hardening rates for different orientations diverge significantly above an engineering strain of 0.10. This divergence led to greater amounts of uniform and total elongation in the 0° orientation for both QP980-B and QP1180-A. In some cases, the minimum strain hardening rate was often distinctive for different orientations, with 0° orientations of QP980-A and QP980-B material having lower strain hardening coefficients at low amounts of strain.

Considering all four replicates, Table II presents a tabulated summary of ultimate tensile strength and uniform elongation along with the associated experimental uncertainties. The replicates exhibited very little variability; experimental errors were approximately 10 MPa for ultimate tensile strength and 0.5 pct for uniform elongation. For different orientations, there was an experimentally significant difference in the uniform elongation for QP980-A and ultimate tensile strength for QP980-B and QP1180-B.

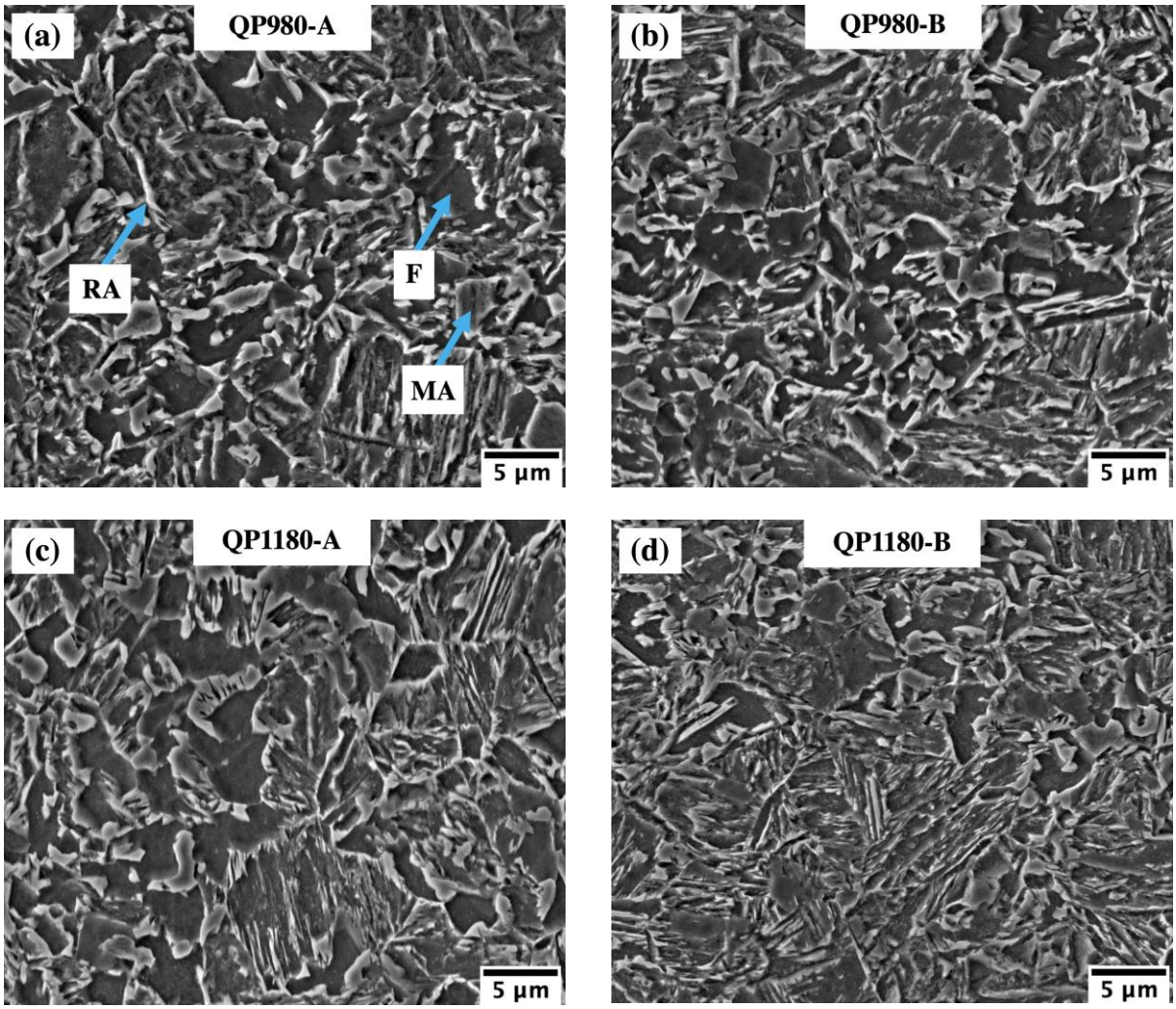

Figure 3: SEM images of (a) QP980-A, (b) QP980-B, (c) QP1180-A, and (d) QP1180-B containing intercritical ferrite (F), martensite-austenite (MA) microconstituents, and dispersed retained austenite (RA).

Serrations in the strain hardening exponent curves were present to various degrees in every steel and orientation tested, particularly at higher amounts of strain. These serrations generally existed with an amplitude of ten percent of the magnitude of the strain hardening exponent, but sometimes existed at a much larger amplitude. For example, large amplitude serrations were present in several cases for QP1180-B; large serrations were observed in zero of four 0° specimens, three of four 45° specimens and two of four 90° specimens. Serrations in strain hardening curves detected in similar steel grades have been described as dynamic strain aging (DSA), caused due to interaction of diffusing solute atoms with dislocation cores[67-69]. De Cooman *et al.* documented such discontinuities, arising due to both TRIP and DSA, with the conclusion that Q&P greatly reduced the magnitude of DSA in comparison to conventional intercritical annealing treatments[69]. Based upon the greater number of large serrations in 45° and 90° orientations of QP1180-B in comparison to 0°, it appears that microstructure orientation may influence DSA, because the amount of solute carbon should be identical for all three orientations.

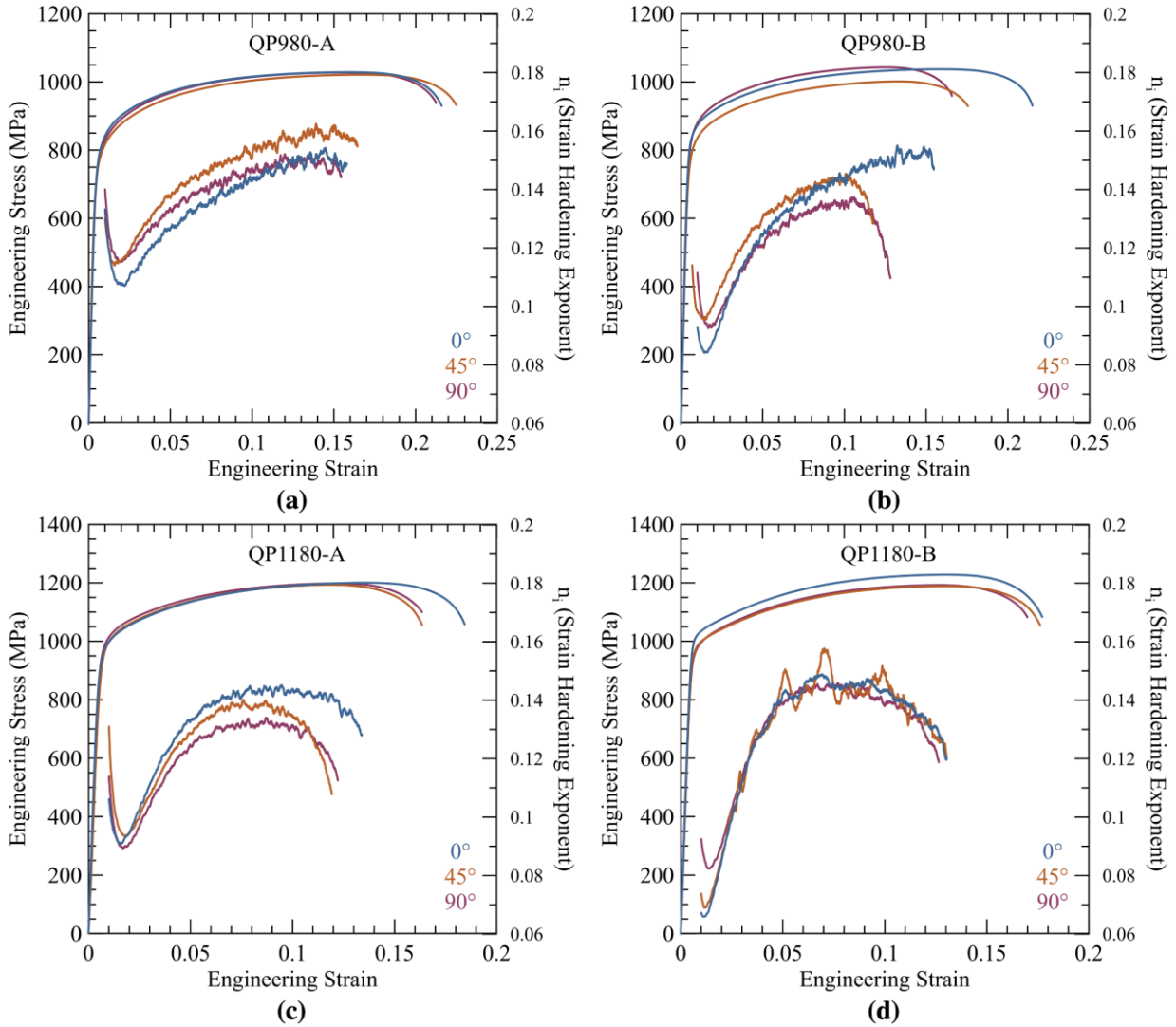

Figure 4: Engineering stress and true strain hardening exponent, n_i, plotted versus engineering strain for (a) QP980-A, (b) QP980-B, (c) QP1180-A, and (d) QP1180-B.

C. Retained Austenite Transformation during Deformation

After straining to failure, XRD scans were performed to quantify retained austenite in both the unstrained grip section and in the uniformly elongated gauge section. XRD scans for each steel and orientation are presented in Figure 5, with computed retained austenite superimposed on the curves. In the unstrained condition, austenite (200) and (220) peaks are easily distinguished. After straining to failure, the amplitude of austenite peaks is significantly diminished relative to the ferrite (200) and (211) peaks. A shoulder is present on the ferrite (211) peak in many conditions, due to inability to distinguish martensite and ferrite peaks because of the small difference in lattice spacings. Solute carbon has been shown to modify the shape of martensite peaks[70], suggesting that varied amounts of solute carbon in tempered and deformation-induced martensite could influence the shape of the peak shoulder. Slight peak broadening due to increased lattice strain was also observed after deformation, which may have smoothed the peak shoulders. Low intensity peaks existing at 2θ values of 25.7° and 31.7° exist in all steels in both unstrained and strained conditions. These peaks are associated with carbides formed during the Q&P treatment.

Deformation-induced retained austenite transformation is inferred by subtracting the retained austenite volume percent in the gauge from retained austenite volume percent in the grip. For example, in the 0° orientation of QP980-A, the unstrained region contains 11.8 volume percent retained austenite, while the gauge region contains 5.1 volume percent retained austenite, suggesting that 6.7 volume percent retained austenite transformed during uniform elongation. All four steels contained a similar amount of retained austenite prior to straining, on the order of 11 or 12 volume percent (Table II). However, transformation exhibits variation for different orientations in the sheet. For QP980-A, QP980-B, and QP1180-B, the greatest amount of transformation occurred in the 0° orientation, while the least transformation occurred in the 90° orientation. Experimental errors associated with these measurements are presented in Table II. Orientation dependence of retained austenite transformation was greater than the error for QP980-A and QP1180-B, but not for QP980-B. In the QP1180-A material, transformation was similar regardless of orientation; measured differences between the three orientations were well within the experimental error.

IV. DISCUSSION

It is understood that austenite transformation is instrumental for improving ductility and formability of AHSS[21,72]. However, the data presented suggest that uniform elongation and UTS are not directly linked to total austenite content or transformation in the Q&P steels investigated here. For example, although the QP980-A and QP980-B steels exhibited tensile strengths slightly greater than 980 MPa in all three orientations, highly variable amounts of retained austenite transformation occurred, ranging from 3.5 to 7.2 volume percent, as shown in Figure 6(a). The 1180 MPa strength level exhibited near-identical behavior, except for a slightly greater amount of austenite transformation. Uniform elongation also showed no clear correlation with austenite transformation (Figure 6(b)). The discovery that total RA transformation is not directly proportional to mechanical performance complements the findings of De Moor *et al.*[45] and others[46-52]. Furthermore, these results suggest that the degree of progressive transformation of retained austenite critically influences mechanical performance, as suggested by Mukherjee *et al.*[53].

In addition to the UTS and uniform elongation, the strain hardening exponent at the UTS was not directly related to the total retained austenite transformation, as is shown in Figure 7(a). Meanwhile, the criterion for strain localization, $\varepsilon = n_i$[19], was clearly adequate for predicting the onset of necking, as is shown in Figure 7(b). Austenite stability models[3] are useful for explaining such behavior. Consider varying retained austenite stability in a Q&P microstructure. In a microstructure containing only unstable retained

austenite, austenite will rapidly transform at low strains, so that at high strain, TRIP will not provide adequate strain hardening to delay the onset of necking. Meanwhile, an optimal microstructure containing a spectrum of austenite stabilities will contribute to strain hardening at the beginning of plastic deformation and effectively suppress necking[34]. In a microstructure containing exceedingly stable austenite, as was the case for all steels investigated here, some austenite did not transform, suggesting that it was not available to improve the ductility via the TRIP-mechanism. Because a substantial quantity of retained austenite remains after deformation, perhaps the uniform elongation could be further enhanced by tailoring austenite stability. Carbides were observed in the form of peaks on the XRD scans, suggesting that composition and processing conditions were insufficient to prevent carbide formation. Perhaps promoting additional carbide formation, either by modifying the heat treatment or reducing the Si content, could decrease austenite stability and increase the amount of austenite available for TRIP. Lower silicon grades processed with the non-isothermal partitioning process have been explored with some success[51, 52, 72].

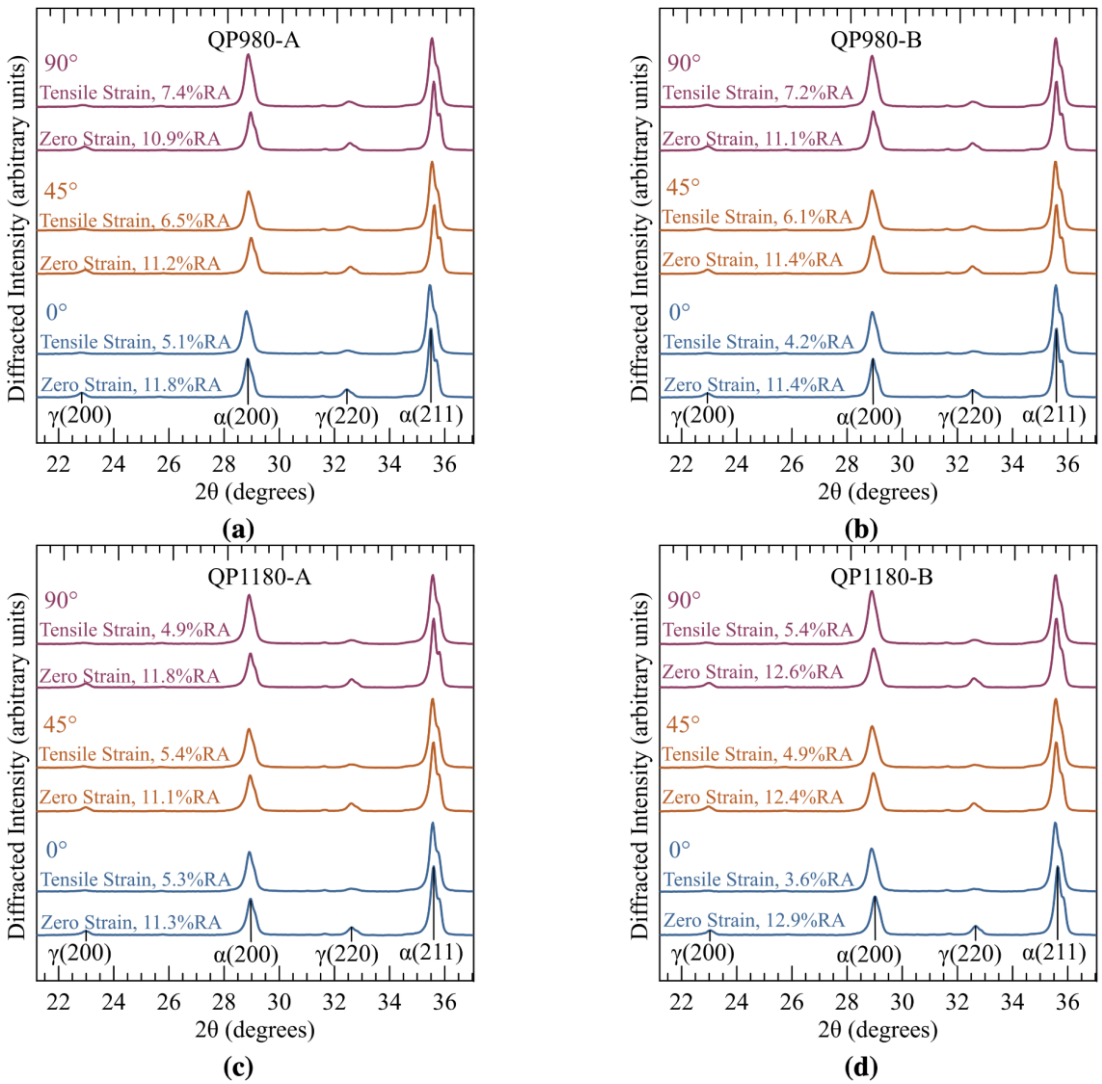

Figure 5: XRD scans of each tensile specimen in the unstrained grip section (labeled "Zero Strain") and the uniformly elongated gauge section after fracture for 0°, 45°, or 90° orientations of (a) QP980-A, (b) QP980-B, (c) QP1180-A, and (d) QP1180-B. Retained austenite (RA) computed by the two-peak method is superimposed on each scan.

Table II: Summary of Tensile Performance and Austenite Transformation with Experimental Error

Steel	**Orientation**	**UTS**	**Uniform Elongation**	**RA at Zero Strain**	**RA at Uniform Tensile Strain**	**RA Transformed**
	degrees	*MPa* *	*pct* *	*vol pct* **	*vol pct* **	*vol pct* ***
QP980-A	0	1017 ± 7	16.3 ± 0.4	11.8 ± 0.3	5.1 ± 0.5	6.7 ± 0.6
	45	1015 ± 6	16.2 ± 0.2	11.2 ± 0.8	6.5 ± 0.9	4.8 ± 1.1
	90	1028 ± 7	15.2 ± 0.1	10.9 ± 0.6	7.4 ± 0.9	3.5 ± 1.1
QP980-B	0	1028 ± 11	15.4 ± 0.8	11.4 ± 0.4	4.2 ± 0.7	7.2 ± 0.8
	45	1008 ± 13	13.2 ± 0.1	11.4 ± 0.4	6.1 ± 0.8	5.3 ± 0.9
	90	1047 ± 5	12.8 ± 0.1	11.1 ± 0.6	7.2 ± 0.5	3.9 ± 0.8
QP1180-A	0	1195 ± 7	13.5 ± 0.3	11.3 ± 0.7	5.3 ± 0.1	6 ± 0.7
	45	1184 ± 6	13.1 ± 0.8	11.1 ± 0.5	5.4 ± 0.1	5.6 ± 0.5
	90	1191 ± 6	12.4 ± 0.3	11.8 ± 0.6	4.9 ± 0.8	6.9 ± 1.0
QP1180-B	0	1225 ± 8	12.7 ± 0.2	12.9 ± 0.9	3.6 ± 0.7	9.3 ± 1.1
	45	1182 ± 6	13.4 ± 0.4	12.4 ± 0.6	4.9 ± 0.0	7.5 ± 0.6
	90	1190 ± 10	12.6 ± 0.1	12.6 ± 0.9	5.4 ± 0.6	7.2 ± 1.0

* Error is the standard deviation of tensile testing data from four replicate tensile specimens

** Error is the standard deviation of RA volume percent measured in three separate orientations on one representative tensile specimen

*** Error is the propagation of uncertainty between RA volume percent at zero strain and after uniform tensile strain

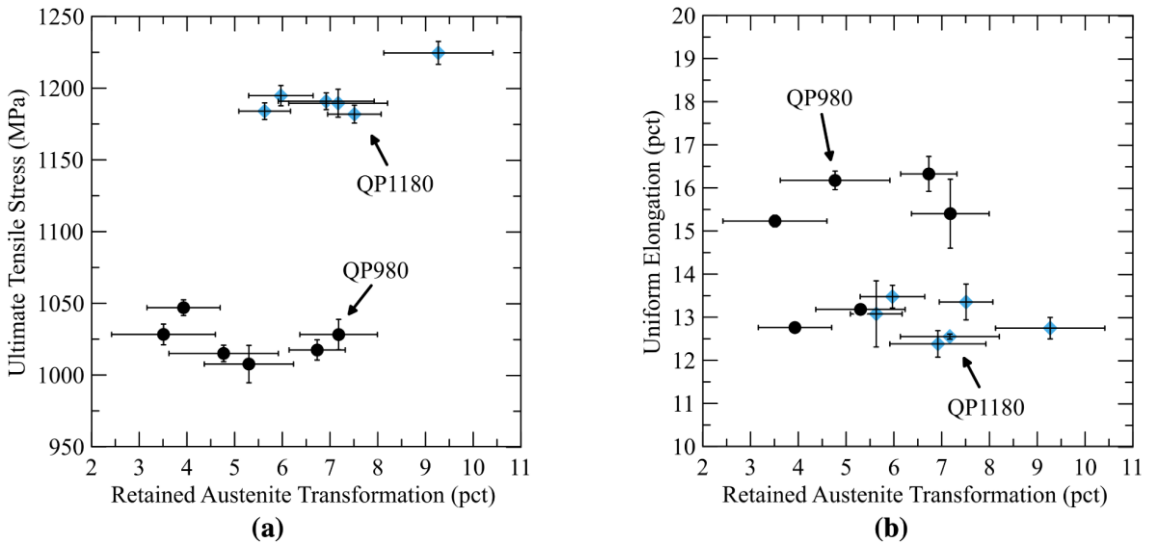

Figure 6: (a) Ultimate tensile stress and (b) uniform elongation plotted versus retained austenite transformation (volume percent) during uniform elongation. All permutations of steel (orientation and heat treatment) for each strength level are plotted concurrently.

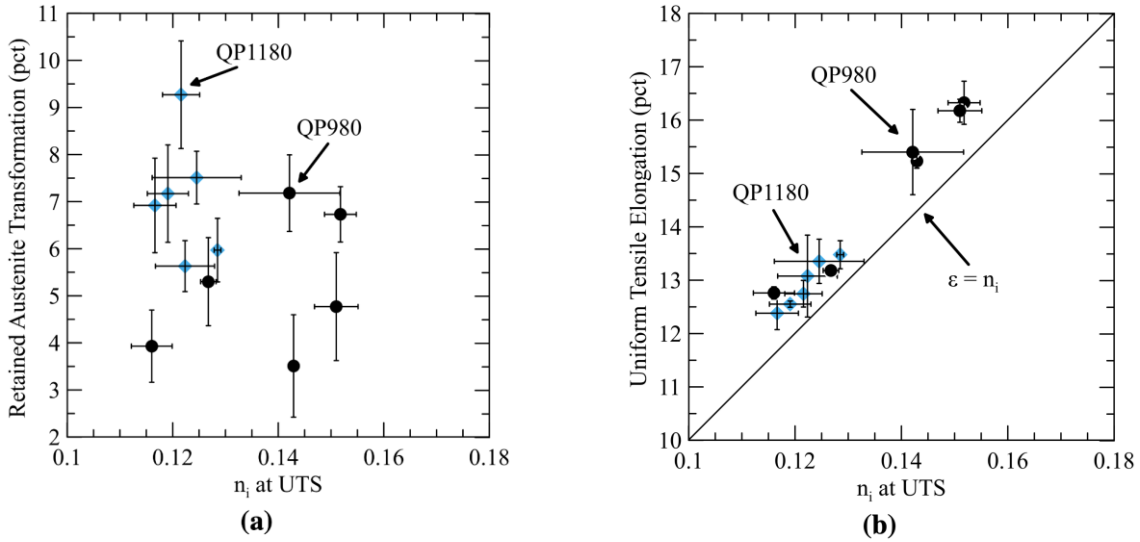

Figure 7: (a) Total retained austenite transformation and (b) tensile elongation plotted versus instantaneous strain hardening exponent, n_i, computed at the onset of necking.

Comparing the transformation behavior among the experimental steels, it appears that some microstructures and orientations contained greater amounts of retained austenite that were available for TRIP at higher strains. These microstructures typically exhibited a strain hardening exponent curve which did not decrease in the final stages of deformation and generally reached a higher uniform elongation. Meanwhile, microstructures that contained less stable retained austenite experienced higher strain hardening rates at the beginning of plastic deformation, and a characteristic decrease in strain hardening near the UTS. Besides TRIP, the relative volume fractions and strain hardening characteristics of ferrite and martensite likely also influenced the strain hardening exponent in these steels. However, a categorical link between mechanical performance and ferrite and martensite volume fraction remains elusive in these data, perhaps because the differences in volume fraction in each steel are only several volume percent. Findley *et al.* showed that the degree of martensite tempering, carbide precipitation, and carbon partitioning critically effects the small strain work hardening behavior, and therefore impacts tensile

ductility[24]. Interestingly, significant variations in small strain work hardening behavior were observed; for instance, QP980-A had a greater small strain work hardening rate than QP980-B, perhaps due to differences in the degree of martensite tempering[73]. Besides work hardening of martensite, multiphase microstructures containing ferrite and martensite exhibit very strong ferrite grain size sensitivity[74, 75], suggesting that small variations in intercritical ferrite grain size could influence work hardening behavior in Q&P steels. Although strain hardening was investigated in tension only, it follows that varied austenite stabilities due to microstructure orientation will affect formability. For materials with varied tensile properties along different orientations, we expect that formability specimen orientation will influence the shape of the forming limit diagram. The challenge of predicting deformation characteristics expands when considering non-monotonic deformation pathways (*e.g.* loading-unloading, bending-unbending, and stretching).

To efficiently utilize TRIP behavior in Q&P microstructures, care must be taken to optimize both the stability and volume fraction of retained austenite. Tailoring the stability may involve designing microstructures that contain a spectrum of austenite stabilities, such that the austenite is available for transformation at all amounts of strain pertinent to sheet forming and crash scenarios. Furthermore, Q&P steel must be characterized such that TRIP is predictable during forming, even while creating complex geometries, such as an automotive B-pillar[76-78], with varying strain rates, temperatures, and strain paths. This characterization should perhaps include: interrupted mechanical testing[64] to elucidate the range of austenite stabilities that exist; formability testing[79] to clarify the role of strain state in TRIP phenomena; and elevated temperature testing[80] to quantify how retained austenite stability is influenced by die heating and processes such as bake hardening, and perhaps adiabatic heating during high-rate deformation[81].

V. CONCLUSIONS

Tension testing, optical and electron microscopy, and x-ray diffraction were used to analyze the role of retained austenite transformation and strain hardening in the mechanical performance of various industrially relevant quenched and partitioned C-Mn-Si steels. These results lead to the following conclusions:

1. In steels with nominally identical composition (e.g. QP980-A and QP980-B), relatively small variations in Q&P processing parameters influenced the transformation of austenite and tensile properties.
2. In all steels, elevated strain hardening rates were achieved by TRIP at high amounts of plastic strain. In some cases, such as QP980-A and QP1180-B, strain hardening rate was consistent regardless of orientation with respect to the rolling direction. Meanwhile, the remaining steels showed differences as a function of orientation that may influence formability.
3. Neither the amount of retained austenite prior to straining nor the total amount of retained austenite transformed during straining were directly correlated to tensile mechanical performance. Meanwhile, in accordance with the instability criterion, the strain hardening rate at necking was directly correlated to uniform elongation. These data suggest that for optimizing formability, tailoring the stability of austenite near strain localization may be more effective than maximizing the volume fraction of austenite.

ACKNOWLEDGEMENTS

The financial support of the Advanced Steel Processing and Products Research Center (ASPPRC) at the Colorado School of Mines, Golden, CO, USA is gratefully acknowledged. CF and KD acknowledge support from the National Science Foundation division of Civil, Mechanical and Manufacturing

Innovation (NSF-CMMI) through award no. 1752530. The authors would like to thank K.X. Steirer, who assisted with X-ray diffraction experiments.

REFERENCES

1 A. Abraham: in *Great Designs in STEEL Seminar*, 2015.
2 Corporate Average Fuel Economy, https://www.nhtsa.gov/laws-regulations/corporate-average-fuel-economy/. Accessed 29 May 2019
3 D.K. Matlock and J.G. Speer: in *International Conference on Micrstructure and Texture in Steels and Other Materials*, A. Haldar, S. Suwas, and D. Bhattacharjee, eds., Springer, Jamshedpur, India, 2008, pp. 185–205.
4 K. Sugimoto, M. Kobayashi, and S. Hashimoto: *Metall. Mater. Trans. A*, 1992, vol. 23, pp. 3085-91.
5 I. Tamura: *Met. Sci.*, 2014, vol. 16, pp. 245–53.
6 H.K.D.H. Bhadeshia: *ISIJ Int.*, 2002, vol. 42, pp. 1059–60.
7 H. Bhadeshia: *Bull. Polish Acad. Sci. Tech. Sci.*, 2010, vol. 58, pp. 255–65.
8 G.B. Olson and C. Morris: *J. Less-Common Met.*, 1972, vol. 28, pp. 107–18.
9 S.S. Hecker, M.G. Stout, K.P. Staudhammer, and J.L. Smith: *Metall. Trans. A*, 1982, vol. 13, pp. 619–26.
10 L.E. Murr, K.P. Staudhammer, and S.S. Hecker: *Metall. Trans. A*, 1982, vol. 13, pp. 627–35.
11 J. Speer, D.K. Matlock, B.C. De Cooman, and J.G. Schroth: *Acta Mater.*, 2003, vol. 51, pp. 2611-22.
12 D. V. Edmonds, K. He, F.C. Rizzo, B.C. De Cooman, D.K. Matlock, and J.G. Speer: *Mater. Sci. Eng. A*, 2006, vol. 438–440, pp. 25–34.
13 J.G. Speer, D. V. Edmonds, F.C. Rizzo, and D.K. Matlock: *Curr. Opin. Solid State Mater. Sci.*, 2004, vol. 8, pp. 219–37.
14 A.M. Streicher, J.G. Speer, D.K. Matlock, and B.C. De Cooman: *International Conference on Advanced High-Strength Sheet Steels for Automotive Applications*, Winter Park, Colorado, 2004, pp. 51-62
15 A.J. Clarke: Colorado School of Mines, 2006.
16 P.J. Gibbs: Colorado School of Mines, 2013.
17 A. Di Schino, C. Braccesi, F. Cianetti, P.E. Di Nunzio, S. Mengaroni, P.R. Calvillo, and J.M. Cabrera: *Mater. Sci. Forum*, 2016, vol. 879, pp. 430–5.
18 J.G. Speer, E. De Moor, K.O. Findley, D.K. Matlock, B.C. De Cooman, and D. V. Edmonds: *Metall. Mater. Trans. A*, 2011, vol. 42, pp. 3591–601.
19 G.E. Dieter: *Mechanical Metallurgy*, 3rd edn., McGraw-Hill, New York, NY, 1961.
20 M. Miles: *ASM Handbook, Formability Anal.*, 2006, vol. 14B, pp. 673–96.
21 S.T. Mileiko: *J. Mater. Sci.*, 1969, vol. 4, pp. 974–7.
22 R. Rana, P.J. Gibbs, E. De Moor, J.G. Speer, and D.K. Matlock: *Steel Res. Int.*, 2015, vol. 86, pp. 1139–50.
23 S. Kang, J.G. Speer, D. Krizan, D.K. Matlock, and E. De Moor: *Mater. Des.*, 2016, vol. 97, pp. 138–46.
24 K.O. Findley, J. Hidalgo, R.M. Huizenga, and M.J. Santofimia: *Mater. Des.*, 2017, vol. 117, pp. 248–56.
25 E. De Moor, S. Lacroix, A.J. Clarke, J. Penning, and J.G. Speer: *Metall. Mater. Trans. A*, 2008, vol. 39, pp. 2586–95.
26 P.J. Gibbs, E. De Moor, M.J. Merwin, B. Clausen, J.G. Speer, and D.K. Matlock: *Metall. Mater. Trans. A*, 2011, vol. 42A, pp. 3691–702.
27 A. Andrade-Campos, F. Teixeira-Dias, U. Krupp, F. Barlat, E.F. Rauch, and J.J. Grácio: *Strain*, 2010, vol. 46, pp. 283–97.

28 M. Mukherjee, S.B. Singh, and O.N. Mohanty, *Materials Science and Technology*, 2007, vol. 23, no. 3, pp. 338-46.
29 J. Min, L.G. Hector, L. Zhang, J. Lin, J.E. Carsley, and L. Sun, *Materials Science and Engineering A*, 2016, vol. 673, pp. 423-29.
30 D. De Knijf, C. Fojer, L. A.I. Kestens, and R. Petrov, *Materials Science and Engineering A*, 2015, vol. 638, pp. 219-27.
31 A.J. Clarke, J.G. Speer, M.K. Miller, R.E. Hackenberg, D. V. Edmonds, D.K. Matlock, F.C. Rizzo, K.D. Clarke, and E. De Moor: *Acta Mater.*, 2008, vol. 56, pp. 16–22.
32 D.T. Pierce, D.R. Coughlin, D.L. Williamson, K.D. Clarke, A.J. Clarke, J.G. Speer, and E. De Moor: *Acta Mater.*, 2014, vol. 90, pp. 417–30.
33 D.T. Pierce, D.R. Coughlin, D.L. Williamson, K.D. Clarke, A.J. Clarke, and J.G. Speer: 2015, vol. 21, pp. 2271–2.
34 C. Chiriac, R. Sohmshetty, J. Balzer, T. Mueller, and J.D. Ju, *IOP Confernce Series: Materials Science and Engineering*, 2018, vol. 418, pp. 1-9.
35 K. Sugimoto, N. Usui, M. Kobayashi, and S. Hashimoto, *ISIJ International*, 1992, vol. 32, no. 12, pp. 1311-18.
36 J. Chiang, B. Lawrence, J.D. Boyd, and A.K. Pilkey, *Materials Science and Engineering A*, 2011, vol. 528, pp. 4516-21.
37 Y. Matsuoka, T. Iwasaki, N. Nakada, T. Tsuchiyama, and S. Takaki, *ISIJ International*, 2013, vol. 53, no. 7, pp. 1224-30.
38 X.C. Xiong, B. Chen, M.X. Huang, J.F. Wang, and L. Wang, *Scripta Materialia*, 2013, vol. 68, pp. 321-24.
39 J. Chiang, J.D. Boyd, and A.K. Pilkey, *Mater. Sci. Eng. A*, 2015, vol. 638, pp. 132-42.
40 P.J. Gibbs, B.C. De Cooman, D.W. Brown, J.G. Schroth, M.J. Merwin, and D.K. Matlock, *Materials Science and Engineering A,* 2014, vol. 609, pp. 323-33.
41 J.H. Ryu, D.I. Kim, H.S. Kim, H.K.D.H. Bhadeshia, and D.W. Suh, *Scripta Materialia*, 2010, vol. 63, pp. 297-9.
42 H. Zhao, W. Li, S. Zhou, and X. Jin, *Metall. Mater. Trans. A*, 2016, vol. 47A, pp. 3943-55.
43 X. Hu, K.S. Choi, X.Sun, Y. Ren, and Y. Wang, *Metall. Mater. Trans. A*, 2016, vol 47A, pp. 5733-49.
44 C.Y. Wang, Y. Chang, J. Yang, W.Q. Cao, H. Dong, and Y. De Wang: *J. Iron Steel Res. Int.*, 2016, vol. 23, pp. 130–7.
45 E. De Moor, J.G. Speer, D.K. Matlock, and D.N. Hanlon: *Mater. Sci. Technol.*, 2011, pp. 568–79.
46 Q. Zhou, L. Qian, J. Tan, J. Meng, and F. Zhang, *Mater. Sci. Eng. A*, 2013, vol. 578, pp. 370-6.
47 R. Blonde, E. Jimenez-Melero, L. Zhao, N. Schell, E. Bruck, S. van der Zwaag, and N.H. van Dijk, *Mater. Sci. Eng. A*, 2014, vol. 594, pp. 125-34.
48 J. Chen, M. Lv, S. Tang, Z. Liu, and G. Wang, *Materials Characterization*, 2015, vol. 106, pp. 108-11.
49 J. Zhang, H. Ding, and R.D.K. Misra, *Mater. Sci. Eng. A*, 2015, vol. 636, pp. 53-9.
50 H. Guo, A. Zhao, R. Ding, C. Zhi, and J. He, *Materials Science and Technology*, 2016, vol. 32, no. 15, pp. 1605-12.
51 X.D. Tan, Y.B. Xu, X.L. Yang, Z.P. Hu, F. Peng, X.W. Ju, and D. Wu, *Materials Characterization*, 2015, vol. 104, pp. 23-30.
52 X.D. Tan, H. He, W. Lu, L. Yang, B. Tang, J. Yan, Y. Xu, and D. Wu, *Mater. Sci. Eng. A*, 2020, vol. 771.
53 M. Mukherjee, O.N. Mohanty, S. Hashimoto. T. Hojo, and K. Sugimoto, *ISIJ International*, 2006, vol. 46, no. 2, pp. 316-24.
54 A.K. De, J.G. Speer, D.K. Matlock, D.C. Murdock, M.C. Mataya, and R.J. Comstock, *Metall. Mater. Trans. A.*, 2006, vol. 37A, pp. 1875-86.
55 G.A. Thomas, J.G. Speer, and D.K. Matlock, *Metall. Mater. Trans. A*, 2011, vol. 42A. pp. 3652-9.

56 L. Wang and W. Feng, in *Advanced Steels: The Recent Scenario in Steel Science and Technology*, eds. Y. Weng, H. Dong, and Y. Gan, 2011, pp. 255-258.
57 Y.J. Li, J. Kang, W.N. Zhang, D. Liu, X.H. Wang, G. Yuan, R.D.K. Misra, and G.D. Wang, *Mater. Sci. Eng. A*, 2018, vol. 710, pp. 181-91.
58 *ASTM Int. E8/E8M-16a*, DOI:10.1520/E0008_E0008M-16A.
59 *ASTM Int. E975-13*, DOI:10.1520/E0975-13.
60 *International Tables for X-Ray Crystallography, Physical and Chemical Tables*, vol. 3, 1962.
61 T. Gnäupel-Herold and A. Creuziger, *Mater. Sci. Eng. A*, 2011, vol. 528, pp. 3594–600.
62 M. Witte and C. Lesch, *Mater. Charact.*, 2018, vol. 139, pp. 111–5.
63 A. Arlazarov, M. Ollat, J.P. Masse, and M. Bouzat, *Mater. Sci. Eng. A*, 2016, vol. 661, pp. 79–86.
64 A. Mostafapour, A. Ebrahimpour, and T. Saeid, *International Journal of ISSI*, 2016, vol. 13, no. 2, pp. 1-6.
65 E.J. Seo, L. Cho, Y. Estrin, and B.C. De Cooman, *Acta Materialia*, 2016, vol. 113, pp. 124-39.
66 A. Navarro-Lopez, J. Hidalgo, J. Sietsma, and M.J. Santofimia, *Materials Characterization*, 2017, vol. 128, pp. 248-56.
67 W. Song, T. Ingendahl, and W. Bleck: *Acta Metall. Sin.*, 2014, vol. 27, pp. 546–55.
68 D.M. Field and D.C. Van Aken: *Metall. Mater. Trans. A*, 2018, vol. 49, pp. 1152–66.
69 B.C. De Cooman, S.J. Lee, S. Shin, E.J. Seo, and J.G. Speer: *Metall. Mater. Trans. A*, 2017, vol. 48, pp. 39–45.
70 L. Xiao, Z. Fan, Z. Jinxiu, Z. Mingxing, K. Mokuang, and G. Zhenqi: *Phys. Rev. B*, 1995, vol. 52, pp. 9970–8.
71 D.K. Matlock and J.G. Speer: in *Microstructure and Texture in Steels and other Materials*, A. Haldar, S. Suwas, and D. Bharracharjee, eds., 2008, pp. 185–205.
72 G.K. Bansal, V. Rajinikanth, C. Ghosh, V.C. Srivastava, S. Kundu, and S. G. Chowdhury, *Metall. Mater. Trans. A*, 2018, vol. 49A, pp. 3501-14.
73 G.A. Thomas, J.G. Speer, D.K. Matlock, G. Krauss, and R.E. Hackenberg, in *International Conference on Martensitic Transformations*, eds. G.B. Olson, D.S. Lieberman, and A. Saxena, 2008, pp. 595-600.
74 Z. Jiang, Z. Guan, and J. Lian, *Mater. Sci. Eng. A*, 1995, vol. 190, pp. 55-64.
75 Y. Bergstrom, Y. Granbom, and D. Sterkenburg, *Journal of Metallurgy*, 2010, pp. 1-16.
76 W. Weib, T. van den Boogaard, E. Till, E. Atzema, M. Grunbaum, and A. Haufe: *Enhanced Formability Assessment of AHSS Sheets*, Luxembourg, 2014.
77 J.N. Hall and J.R. Fekete: *Steels for Auto Bodies: A General Overview*, Elsevier Ltd, 2016.
78 D. Kitting, A. Ofenheimer, A.H. van den Boogaard, and P. Dietmaier: *Key Eng. Mater.*, 2013, vol. 554–557, pp. 1252–64.
79 E.H. Atzema: *Formability of Auto Components*, 2016.
80 J. Coryell, V. Savic, L. Hector, and S. Mishra: *SAE Int.*, DOI:10.4271/2013-01-0610, 2013.
81 C. Finfrock, C. Becker, T. Ballard, G. Thomas, K. Clarke, and A. Clarke, *Contributed Papers from Materials Science & Technology*, Portland, Oregon, 2019, pp. 1236-43.